Transforming a volcanic rock powder waste into an efficient adsorbent to remove dyes (acid green 16 and acid red 97) and metals (Ag$^+$, Co^{2+}, and Cu^{2+}) from water

Diovani L. Rossatto[1] · Rachel de Lima[1] · Matias S. Netto[1] · Julien Vieillard[2] · Luis F. O. Silva[3] · Diana Pinto[3] · Guilherme L. Dotto[1,2]

Abstract

This study searched for the best synthesis route for producing an adsorbent from the alkaline fusion of volcanic rock powder waste. The samples synthesized under different conditions of temperature and alkalizing ratio/precursor material, nine in total (NP.F, NP.F1, NP.F2, ...NP.F8), were used in the adsorption of acid green 16 (AG 16) and acid red 97 (AR 97) dyes and Ag$^+$, Co^{2+}, and Cu^{2+} ions. Subsequently, the 2^2 central composite rotational design (CCRD) was applied, and the effects of the alkalizing ratio (NaOH)/volcanic rock (VR) and temperature (T) on the synthesis process were analyzed in terms of their influence on the physical properties of the materials and in the process of adsorption of contaminants. From the experimental design, it can be seen that the independent variables alkalizing ratio/volcanic rock and temperature greatly influence the characteristic and synthesis of adsorbent materials by alkaline fusion, which in turn reflects on the results achieved in the adsorption of contaminants. Therefore, the temperature of 550 °C and NaOH/VR ratio equal to 1 was the most satisfactory synthesis route to obtain high values of adsorption capacity (q, mg g^{-1}) and removal (R, %) for all studied contaminants, as well as the optimization of the physical characteristics of the material. For example, the adsorption capacity of dye AG 16 was 49.1 mg g^{-1}, and for Ag$^+$ was 66.2 mg g^{-1}, while the removal percentages were 97.6% and 93.4%, respectively. This approach made it possible to transform volcanic rock powder wastes into an efficient adsorbent to treat contaminated waters with dyes and metals.

Keywords Experimental design · Adsorbent · Adsorption · Volcanic rock · Alkaline activation · Alkaline fusion

Introduction

The mineral extraction process from precious stones, basaltic rock, or other minerals generates considerable volcanic rock powder waste. This approach implies costs for the generating company, which must treat and dispose of this waste properly and thus mitigate environmental damage as much as possible. The state of Rio Grande do Sul is an important Brazilian producer of semi-precious stones (agate, amethyst) and rocks for the most diverse areas of civil construction (Hartmann et al. 2015). Nova Prata, the basalt capital of Brazil, generates around 10,000 tons per year of volcanic rock dust waste from the extraction of basaltic rock (Rossatto et al. 2022), which is usually stored in the open (Pinto and Hartmann 2011).

Most of the time, the waste of volcanic rock is stored on the slopes of open mines. These can reach water bodies through their fragmentation and transport through

✉ Guilherme L. Dotto
guilherme_dotto@yahoo.com.br

1 Research Group on Adsorptive and Catalytic Process Engineering (ENGEPAC), Federal University of Santa Maria, Av. Roraima, 1000-7, 97105–900, Santa Maria, RS, Brazil

2 Normandie Université, UNIROUEN, INSA Rouen, CNRS, COBRA (UMR 6014), 27000 Evreux, France

3 Department of Civil and Environmental, Universidad de La Costa, CUC, Calle 58 # 55–66, Atlántico, Barranquilla, Colombia

rainwater and thus contaminate them (Ontiveros-Cuadras et al. 2018). When these materials enter the aquatic environment, they are susceptible to complexation, precipitation, and adsorption. As a result, they tend to decant, becoming part of the sediments (Remor et al. 2018). According to Pejman et al. (2015) and Silva et al. (2016), sediment contamination by chemical species, such as nutrients and metals, due to their bioaccumulation, bioavailability, persistence, and possible toxicity threatens aquatic ecosystems. Furthermore, in mining regions, the concentrations of elements or chemical compounds in the sediments of water bodies are higher than the background levels of chemical species and, therefore, may pose risks to ecosystems (Vosoogh et al. 2016). Therefore, there is an increasing search for the efficient application of mined materials to eliminate or reduce the impacts caused to the environment.

Nowadays, alkaline-activated materials, such as mesoporous geopolymers, have been attracting space in research focused on adsorption, and favorable results have been achieved in treating effluent-containing dyes (Vieira et al. 2021). Due to the composition of volcanic rock powder, research has sought to investigate its capacity as an adsorbent, either functionalized/activated with another element or applied directly. Chao et al. (2019) prepared a volcanic rock-based ceramsite adsorbent material for fluorine removal. At 298 K, the adsorption capacity of fluorine was 10.16 mg g^{-1}. Bugarčić et al. (2018) already sought to define the adsorbent potential of raw volcanic rock powder for heavy metals in anionic form. The adsorption capacities for As, Cr, and Se were 12.6, 15.6, and 9.29 mg g^{-1}, respectively. In this sense, alkaline fusion is a thermal treatment that occurs in the presence of alkaline compounds at temperatures higher than their fusion points (Demir et al. 2019). This transformation route allows the amorphization of the material, thus causing an increase in surface area and generating interesting physicochemical properties of the final material (Wei, Ning et al. 2014). This technique has already been synthesized in different materials and successfully used in the adsorption of a variety of pollutants (Demir et al. 2019; Wajima et al. 2011; Monzón et al. 2019; Hwang et al. 2019; Tchakoute et al. 2013; Tchadjié et al. 2016).

Rossatto et al. (2022) demonstrated the adsorbent potential of raw volcanic rock powder and alkaline activated with NaOH for dyes acid green 16 (AG 16) and acid red 97 (AR 97), and metallic ions silver (Ag$^+$), cobalt (Co^{2+}), and copper (Cu^{2+}). Given this, this article seeks to obtain the best synthesis route, through experimental planning, for the alkaline fusion of volcanic rock tailings from Nova Prata, evaluating the effects of the alkalizing ratio (NaOH) and volcanic rock and temperature on the synthesis process. So, it is possible to transform this waste into an alternative adsorbent with better features.

Material and methods

Materials, contaminants, and chemicals

Supplementary file.

Synthesis, experimental design, and physical characteristics of the samples

Preliminarily, the NaOH was ground manually, and subsequently, the volcanic rock powder samples were mixed, and a sufficient amount of deionized water to form a paste was added. Then, the samples were subjected to heat treatment in a muffle (alkaline fusion) for 90 min. Soon after, the samples were washed with deionized water and filtered under vacuum until neutral pH, and finally, they were dried in an oven at 90 °C for 8 h, thus obtaining the new materials. The adsorbent synthesis procedure is shown in Fig. 1.

The effects of temperature (T) and mass ratio between the alkalizing agent NaOH and the volcanic rock (RV) were studied using a central composite rotational design 2^2 (CCRD) containing three central and four axial points. As responses to this planning, the dependent variables were the adsorption capacity, q (mg g^{-1}), the removal capacity, R (%), and the physical characteristics of the materials (specific surface area, SSA in m^2 g^{-1}, average pore diameter, APD in nm and total pore volume, TPV in cm^3 g^{-1}). The Fischer test determined the models' prediction, while the coefficient of determination (R^2) explained the variance. Statistica 8.0 software (StatSoft, USA) was used to analyze the results. Table 1S (Supplementary information) shows the operational conditions of the materials synthesis through the coded matrix, the real values, and the independent variables of the experimental design.
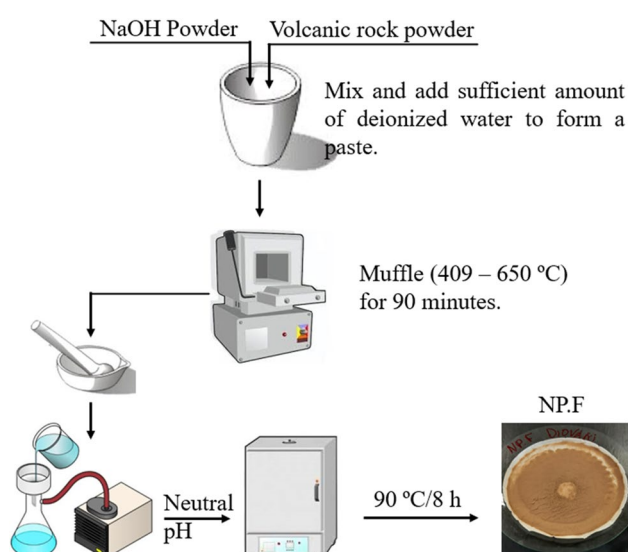

Fig. 1 The adsorbent synthesis procedure

Table 1 Experimental design 2^2 matrix and physical properties of the studied samples

Run	Samples	T (°C)	Mass ratio NaOH/VR	SSA (m² g⁻¹)	APD (nm)	TPV (cm³ g⁻¹)
1	NP.F1	650 (+1)	1.5 (+1)	133.30	7.03	0.253
2	NP.F2	650 (+1)	0.5 (-1)	7.92	14.56	0.029
3	NP.F3	450 (−1)	1.5 (+1)	64.74	10.49	0.170
4	NP.F4	450 (−1)	0.5 (−1)	15.82	11.05	0.044
5	NP.F5	691 (+1.41)	1.0 (0)	98.91	7.68	0.190
6	NP.F6	409 (−1.41)	1.0 (0)	147.76	16.00	0.191
7	NP.F7	550 (0)	1.705 (+1.41)	40.08	11.83	0.119
8	NP.F8	550 (0)	0.295 (−1.41)	5.55	12.77	0.018
9	NP.F	550 (0)	1 (0)	39.99	11.76	0.118
10	NP.F	550 (0)	1 (0)	39.99	11.76	0.118
11	NP.F	550 (0)	1 (0)	39.99	11.76	0.118

VR = volcanic rock

The physical characteristics of the samples, pore volume, pore size distribution, and specific surface area were determined by the Brunauer-Emmett-Teller (BET) and Barret-Joyner-Halenda (BJH) methods (Brunauer et al. 1938). The instrumental method is described in the "Supplementary information."
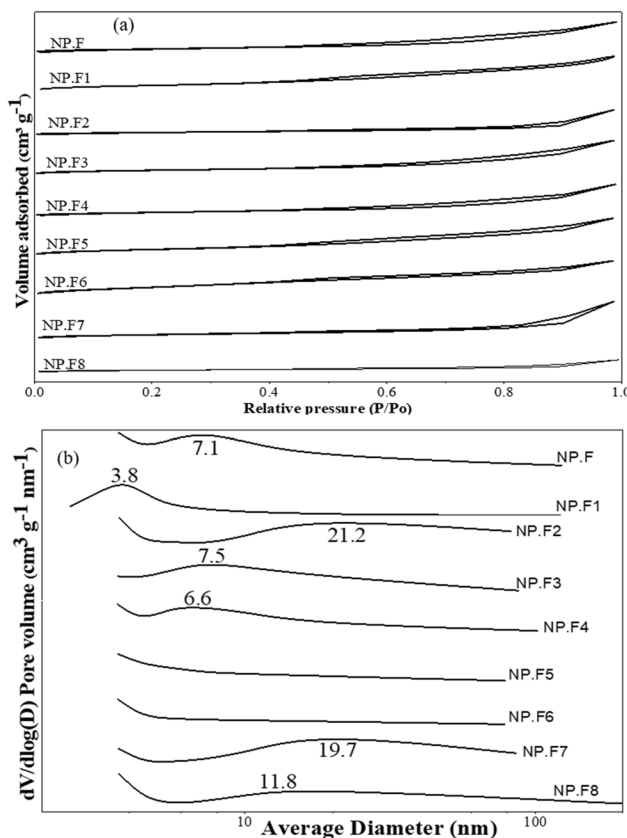

Fig. 2 **a** N₂ adsorption-desorption isotherms and **b** pore size distribution of the materials

Adsorptive studies

Batch adsorption tests were carried out to investigate the ability of the synthesized materials to remove and adsorb contaminants from aqueous solutions and thus determine the effects of temperature (T, °C) and the alkalinizing/volcanic rock ratio (NaOH/RV ratio) in the synthesis of the samples. The adsorption operations were carried out under the following operational conditions: initial concentration of the contaminant of 50 mg L⁻¹, solution volume of 25 mL, a fixed adsorbent dosage of 1 g L⁻¹, stirring speed of 150 rpm, temperature of 25 °C, and 2-h adsorption. The tests were carried out in a bath tank with Dubnoff Orbital water (Nova, Brazil) with digital temperature control. Initially, aqueous solutions were prepared (stock solutions, 1.00 g L⁻¹) of the contaminants of AG 16 and AR 97 dyes, of Ag^+ (silver nitrate, $AgNO_3$), Co^{2+} (cobalt II chloride,
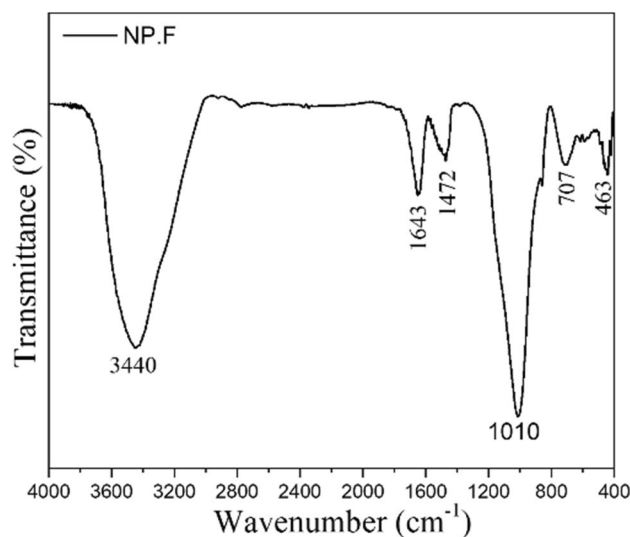

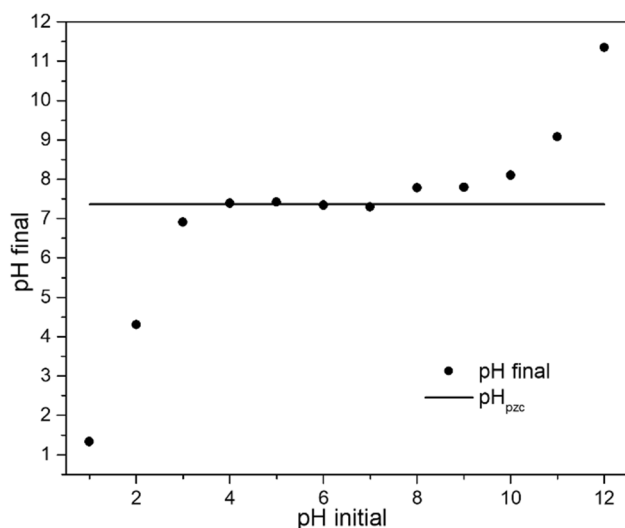**Fig. 3** FTIR spectra synthesized material NP.F

Fig. 4 Plot used to determine the point of zero charge of the NP.F sample

CoCl$_2$), and Cu^{2+} (sulfate of copper (II), CuSO$_4$), and, later, the experiments were carried out by diluting the stock solution in deionized water until the working concentration. According to preliminary tests, the pH of the aqueous dye solutions was 2.3, while the pH of the metals was that of the solution itself (copper = 5.98, cobalt = 6.45, and silver = 6.53). The experiments were carried out in triplicate.

At the end of each adsorption test, samples were collected, filtered, or centrifuged; finally, the residual concentration of the contaminant in the solution was measured. An Agilent Technologies atomic absorption spectrophotometer, model 240 FS AA, was used for metals. A Kasuaki UV-VIS spectrophotometer, model IL-226-NM, was used for the dyes. From the final concentrations of the pollutants after the adsorption process obtained in the spectrophotometric analyses, the adsorption capacity (q, mg g^{-1}) and the removal efficiency (R, %) were calculated and used to evaluate the adsorption. Equations (1) and (2) were used to determine the adsorption capacity and removal capacity, respectively:

$$q = \frac{(C_0 - C_r)V}{m} \tag{1}$$

$$RE = \frac{(C_0 - C_r)\,100}{C_0} \tag{2}$$

where C_0 is the initial concentration of the contaminant in the solution (mg L^{-1}), C_r is the residual concentration of the contaminant in the solution (mg L^{-1}), V is the volume of the solution (L), and m is the amount of adsorbent (g).
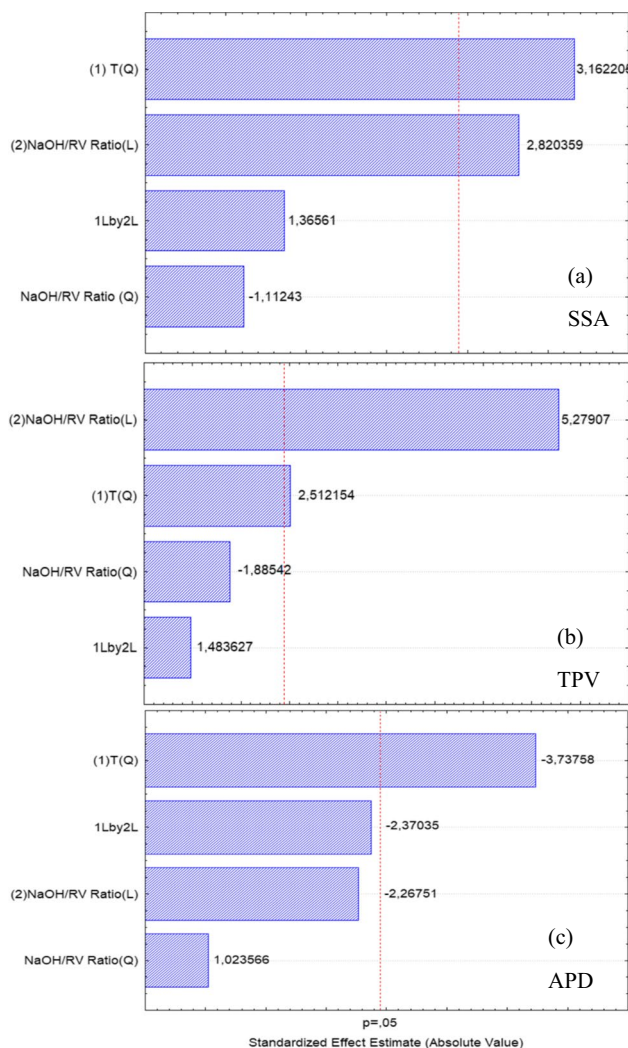
Fig. 5 Pareto charts for the responses: **a** specific surface area (SSA), **b** total pore volume (TPV), and **c** average pore diameter (APD) for the NP.F

Results and discussion

Physical and chemical characteristics of the samples

The physical properties of the samples synthesized and studied in this article are reported in Table 1 from the coded matrix, the real values, the independent variables, and responses of the CCRD 2^2 experimental design. The physical characteristics, specific surface area, average pore diameter, and total pore volume of adsorptive materials can indicate the probability of the material being a good adsorbent. The higher their values are, the better the adsorption capacity of the material (Hosseinzadeh et al. 2015).

Figures 2a and b represents the N$_2$ adsorption and desorption isotherms and the pore size distributions of the materials, respectively. According to IUPAC, the isotherms of

Fig. 6 Response surfaces for **a** specific surface area (SSA), **b** average pore diameter (APD), and **c** total pore volume (TPV)
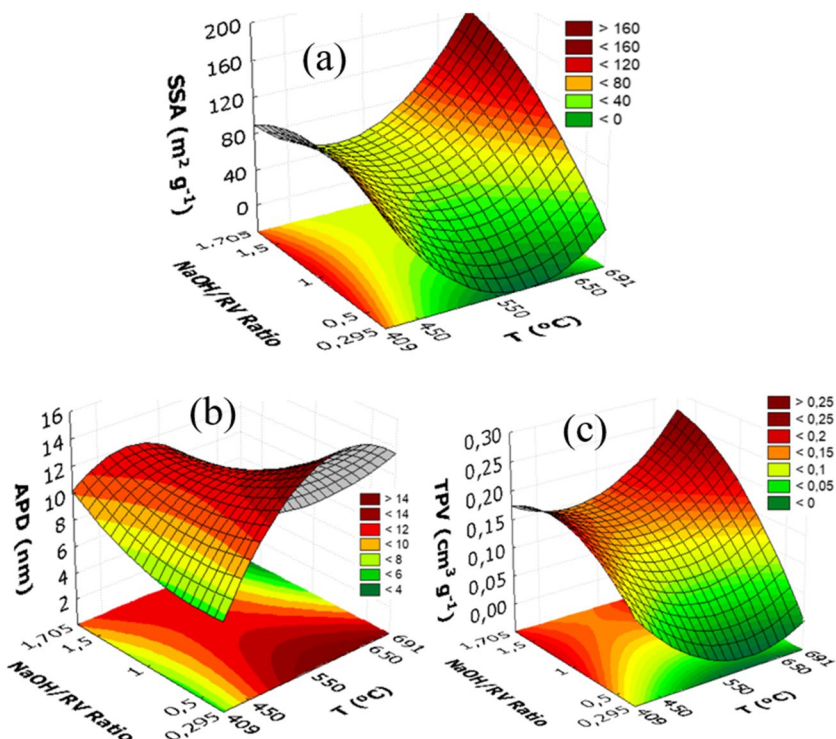

Fig. 2a are classified as type IV and with a hysteresis loop in the H3 format, indicating the existence of mesopores (Thommes 2010). In addition, the asymptotic vertical profile for high P/P_0 values in all samples suggests that the structures are meso- and macroporous with non-uniform size and slit-shaped pores (Wdowin et al. 2014). Already by observing Fig. 2b, it is possible to verify the dominant presence of mesopores (2 nm ≤ pore diameter ≤ 50 nm) in all samples, which corroborates what was predicted by the N_2 adsorption-desorption isotherms and a small incidence of macropores.

Figure 3 presents the FTIR spectrum of the NP.F sample. The 3440 cm^{-1} broadband is attributed to O–H flexion and elongation of the silanols and also of the remaining adsorbed water. The absorption band at 1643 cm^{-1} represents the H–O–H bending vibrations of bound water molecules, which can be absorbed by the surface and trapped in the material structure after adsorption of atmospheric water in the cooling of volcanic magma. The weak band at 1472 cm^{-1} is due to O–C–O stretching vibrations, indicating the presence of sodium bicarbonate (Na_2CO_3), which suggests the occurrence of atmospheric carbonation after alkaline melting. The

Table 2 Experimental design 2^2 matrix and responses for the adsorption tests on dyes AG 16 and AR 97

Run	Samples	T (°C)	Mass ratio NaOH/VR	AG 16		AR 97	
				R (%)[a]	q (mg g^{-1})[a]	R (%)[a]	q (mg g^{-1})[a]
1	NP.F1	650 (+1)	1.5 (+1)	97.7±0.1	49.2±0.1	98.4±0.2	49.2±0.3
2	NP.F2	650 (+1)	0.5 (−1)	95.1±0.3	47.9±0.3	96.3±0.1	48.1±0.2
3	NP.F3	450 (−1)	1.5 (+1)	99.2±0.1	49.9±0.1	98.8±0.1	49.4±0.1
4	NP.F4	450 (−1)	0.5 (−1)	94.1±0.1	47.4±0.1	97.4±0.1	48.7±0.1
5	NP.F5	691 (+1.41)	1.0 (0)	99.2±0.2	49.9±0.3	96.7±0.3	48.3±0.1
6	NP.F6	409 (−1.41)	1.0 (0)	99.0±0.4	49.8±0.1	96.9±0.1	48.4±0.3
7	NP.F7	550 (0)	1.705 (+1.41)	99.7±0.1	49.9±0.1	97.7±0.4	48.9±0.1
8	NP.F8	550 (0)	0.295 (−1.41)	94.1±0.2	47.4±0.3	97.1±0.1	48.6±0.1
9	NP.F	550 (0)	1 (0)	97.6±0.1	49.1±0.2	91.4±0.1	45.7±0.2
10	NP.F	550 (0)	1 (0)	97.6±0.1	49.1±0.2	91.4±0.1	45.7±0.2
11	NP.F	550 (0)	1 (0)	97.6±0.1	49.1±0.2	91.4±0.1	45.7±0.2

VR = volcanic rock. A mean ± standard error for n=3. Coded values are in brackets
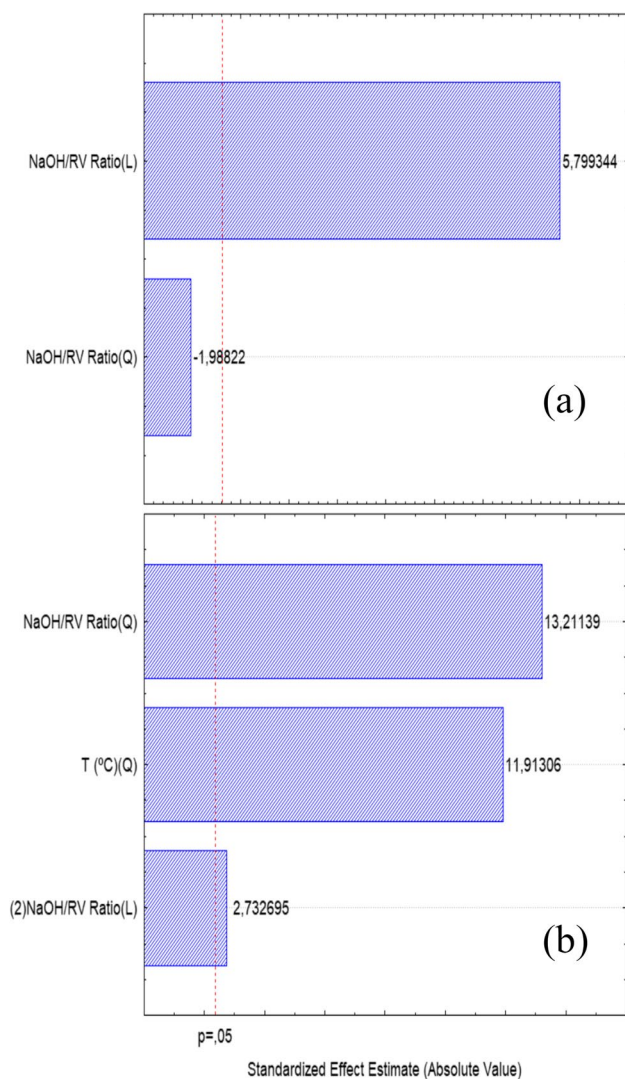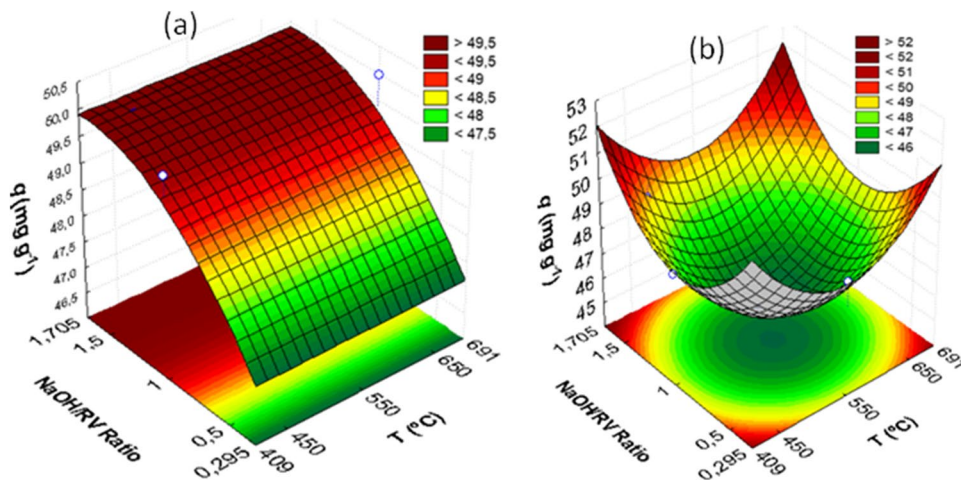
Fig. 7 Pareto charts for the adsorption capacity response of the acid green 16 (**a**) and acid red 97 (**b**) dyes

Fig. 8 Response surfaces for the adsorption capacity, q (mg g^{-1}) of the dyes **a** AG 16 and **b** AR 97

vibration band 1010 cm^{-1} is relative to the Si–O–T asymmetric elongation (T:Al or Si), indicating the amorphous aluminosilicate gel phase. The band at 707 cm^{-1} is related to bending vibrations –Si–O–Si– in (SiO$_2$)$_n$ molecules, and in this band, there are differences between different silica compounds, such as quartz and cristobalite, and on account of the alkaline melting process can be attributed to the formation of amorphous to semi-crystalline aluminosilicate materials. Finally, the 463 cm^{-1} band is characteristic of the tectosilicate network's Si–O stretching vibrations.

The point of zero charge (pH$_{pzc}$) is an important parameter that allows predicting the charge on the surface of the adsorbent as a function of pH and, therefore, evaluating the effect of pH on the adsorption process, as well as assisting in the choice of adsorbate and pH that it can be adsorbed by the adsorbent under study. The pH$_{pzc}$ is the pH where the charge on the positive surface sites is equal to that on the negative sites (zero charge on the surface of the adsorbent). The solution's adsorbent surface is negatively charged when the pH is higher than pH$_{pzc}$. It can interact with positive species, while at pH lower than pH$_{pzc}$, the solid surface is positively charged and can interact with negative species. The methodology used in this work is called the "11 points experiment". The procedure consisted of mixing 20 mg of the adsorbent in 20 mL of 0.1 M NaCl under 11 different initial pH conditions, ranging from 1 to 12 at intervals of 1 in 1. The pH adjustments were made with 0.1 HCl M and 0.1 M NaOH, stirring at 150 rpm with pH measurement after 24 h. The results were presented relating the final pH versus initial pH (Fig. 4). The value referring to pH$_{pzc}$ corresponds to the range in which the final pH remains constant regardless of the initial pH. The zero charge point (pHzcp) of NP.F was 7.4, obtained from the arithmetic mean of the points that remained constant for the final pH.

Pareto charts were used to verify whether the independent variables (linear and quadratic), and their interaction were significant in the responses. The Pareto charts for the

Table 3 Comparison of the adsorption capacity of several adsorbents used in the adsorption of the contaminants studied in this article

Adsorbent	Adsorbate	pH	T (K)	q (mg g^{-1})	References
Low-moor Peat and Smectite	AG dye	5.67	298	13.1	
Shells of bittin		2-8	318	7.0	(Aydin and Baysal 2006)
ZrO$_2$/CeO$_2$ nanocomposite		3	293	43 a 74.5	(Ali et al. 2021)
ZnS:Cu nanoparticles		3.2	-	38.6	(Masoudian et al. 2018)
Magnetic chitosan nanocomposite		5.4	298	26.2	
Activated *Prunus dulcis*		2	323	50.8	
NP.F		2.3	298	49.1	This work
Citrus limonum peels	AR dye	2	303	0.6	
Activated carbon from fibrous		2	298	21.7	
Activated carbon		-	298	55.2	
Rice wine lees		5	298	18.7	Wang et al. (2020)
Magnetic nano-Fe$_3$O$_4$		5	303	40.2	Xing et al. (2014)
Chitosan		7	298	8.2	Jia et al. (2019)
NP.F		2.3	298	45.7	This work

responses of specific surface area (SSA), total pore volume (TPV), and average pore diameter (APD) are represented in Fig. 5a, b, and c, respectively. Negative values on the graph indicate that the independent variables are inversely proportional to the dependent variables, and positive values show that the independent variables are directly proportional to the response. The red line (p=0.05) indicates significance. When the independent variables are significant, their respective columns cross the red line. Regarding SSA (Fig. 5a) and TPV (Fig. 5b), it was found that the linear effect of the NaOH/RV ratio and the quadratic effect of temperature (T) were significant (p<0.05). The positive sign of these significant effects shows that both SSA and TPV increase with increasing T and NAOH/RV ratio. In the case of APD (Fig. 5c), only T's quadratic effect was significant.

Table 2S presents the equations obtained in the statistical analysis for the response's specific surface area, average pore diameter, total pore volume, and statistical parameters.

Again, the 95% confidence interval ($p < 0.05$) was used in statistical studies.

So that the statistical equations in Table 2S satisfactorily represent the experimental data, they must be significant, predictive, and reliable (Myers and Montgomery 2009). The significance of the mathematical models can be verified by the high values of the determination coefficient shown in Table 2S ($R^2 > 0.80$). Furthermore, the values obtained for Fischer" F confirmed that the polynomial models were predictive (Table 3S). Because of this, it can be stated that the mathematical models were significant, predictive, and reliable, thus representing the SSA, APD, and TPV responses. Considering that the equations were significant, predictive, and reliable, the response surfaces were plotted to represent SSA, APD, and TPV as a function of temperature (T) and mass ratio between alkalinizing NaOH and volcanic rock (RV). These surfaces are shown in Figure 6.

Table 4 Experimental design 2^2 matrix and responses for the adsorption tests on metallic ions (Ag$^+$, Co^{2+}, and Cu^{2+}).

Run	Samples	T (°C)	Mass ratio NaOH/VR	Ag$^+$		Co^{2+}		Cu^{2+}	
				R (%)[a]	q (mg g^{-1})[a]	R (%)[a]	q (mg g^{-1})[a]	R (%)[a]	q (mg g^{-1})[a]
1	NP.F1	650 (+1)	1.5 (+1)	93.5±0.2	46.7±0.1	46.3±0.1	23.1±0.1	76.5±0.2	38.2±0.1
2	NP.F2	650 (+1)	0.5 (−1)	98.0±0.2	49.0±0.1	40.8±0.1	20.4±0.1	81.8±0.3	40.9±0.1
3	NP.F3	450 (−1)	1.5 (+1)	86.4±0.1	43.2±0.3	36.9±0.2	18.4±0.4	61.7±0.1	30.9±0.2
4	NP.F4	450 (−1)	0.5 (−1)	90.2±0.1	45.1±0.1	32.4±0.3	16.2±0.3	56.5±0.3	28.3±0.1
5	NP.F5	691 (+1.41)	1.0 (0)	93.2±0.3	46.6±0.2	47.5±0.1	23.8±0.1	77.5±0.1	38.8±0.1
6	NP.F6	409 (−1.41)	1.0 (0)	87.4±0.1	43.7±0.2	46.7±0.1	23.4±0.2	79.1±0.2	39.6±0.3
7	NP.F7	550 (0)	1.705 (+1.41)	89.6±0.2	44.8±0.1	40.4±0.4	19.3±0.1	79.7±0.4	39.9±0.4
8	NP.F8	550 (0)	0.295 (−1.41)	98.3±0.1	49.1±0.4	30.6±0.3	15.3±0.3	70.1±0.2	35.1±0.3
9	NP.F	550 (0)	1 (0)	93.4±0.1	46.7±0.1	63.1±0.1	31.6±0.2	97.1±0.2	48.5±0.1
10	NP.F	550 (0)	1 (0)	93.4±0.1	46.7±0.1	63.1±0.1	31.6±0.2	97.1±0.2	48.5±0.1
11	NP.F	550 (0)	1 (0)	93.4±0.1	46.7±0.1	63.1±0.1	31.6±0.2	97.1±0.2	48.5±0.1
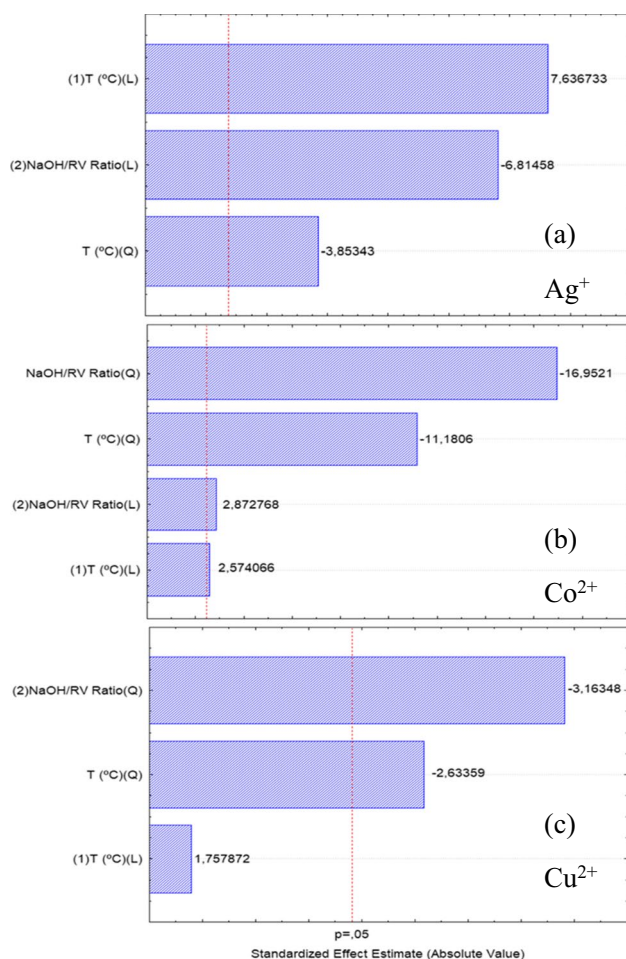
Fig. 9 Pareto charts for the adsorption capacity response of the metallic ions Ag^+ (**a**), Co^{2+} (**b**), and Cu^{2+} metallic ions by the NP.F

It can be seen that the specific surface area increases as T and the NaOH/RV ratio increase successively, assuming the maximum values for T equal to 691 °C and NaOH/RV ratio of 1.705 (Fig. 6a). On the other hand, the SSA response also assumes high values by keeping T at 409 °C and varying the NaOH/RV ratio, with the maximum value reached for the ratio equal to 1. The total pore volume (Fig. 6c) shows a similar trend. According to Choi et al. (2014), the pore volume increases due to Ca and Si compounds on the surface of the volcanic rock that reacts with HO, leading to calcium hydroxide and silanol formation. So, it can be suggested that the improvement of the specific surface area and the total pore volume of the material depends mainly on the alkalizing/volcanic rock ratio in the material synthesis. On the other hand, in Fig. 6b, the mean pore diameter tends to increase and reach the highest values as T increases and the NaOH/RV ratio is maintained at 0.295, so it can be said that the improvement in the mean pore diameter is linked mainly to T synthesis. As Duxson et al. (2007) claimed, the alkaline hydrothermal reaction of different aluminosilicate materials

results in the formation of various structures, which depend on the reaction conditions, such as temperature, alkaline cation, and Si/Al ratio.

Adsorption results

Adsorptive tests were carried out with the newly synthesized materials. The experimental data were statistically analyzed (CCRD 2^2) to verify the influence of temperature and the NaOH/RV ratio of materials synthesis on the adsorption of acid green 16 (AG 16) and acid red 97 (AR 97) dyes and metallic ions (Ag^+, Co^{2+}, and Cu^{2+}). Thus, we can define the best synthesis route for the materials.

Dyes adsorption

The coded matrix, real values, independent variables, and responses are shown in Table 2. The confidence interval used in the statistical analysis was 95% ($p < 0.05$). Table 5 shows the statistical parameters for the equations determined in the statistical study of the dependent variables removal efficiency (R, %) and adsorption capacity (q, mg g^{-1}).

The Pareto charts for the adsorption capacity response (q, mg g^{-1}) for the adsorption of acid green 16 and acid red 97 dyes are represented in Fig. 7a and b, respectively. It was found that the linear variable of the NaOH/RV ratio was significant in both dyes. In contrast, the quadratic effect of the NaOH/RV ratio and T were only significant for the AR 97 dye, and the quadratic effects were positive, also indicating a minimum point for q.

The significance of the polynomial models obtained through the high values of the coefficient of determination ($R^2 > 0.83$) is verified (Table 3S). Furthermore, the evaluation of the calculated and tabulated values for Fischer's F confirmed that the mathematical models were predictive (Table 3S). Given this, it can be stated that the model equations found in the statistical study were significant, predictive, and reliable, thus representing the experimental data of the R and q responses. These are represented in Fig. 8 from the response surfaces of the experimental design for the dependent variable q.

From Fig. 8a, it can be verified that the T of the synthesis of the materials does not influence the adsorption process of the dye AG 16. On the other hand, the NaOH/RV ratio has a strong relationship with the improvement in the adsorptive capacity of the materials, which reach values maximum q (mg g^{-1}) when the alkalizing/volcanic rock ratio is equal to 1.705 ($R = 99.7$ % and $q = 50.2$ mg g^{-1}). In turn, the adsorption of the dye AR 97 has its values optimized when the T and the alkalinizing/volcanic rock ratio of synthesis of the samples are located close to the axial points of the experimental planning, being the maximum value found for the adsorption capacity and of removal when T = 450 °C

Fig. 10 Response surfaces for the adsorption capacity, q (mg g^{-1}) of the metallic ions **a** Ag$^+$, **b** Co^{2+}, and **c** Cu^{2+}
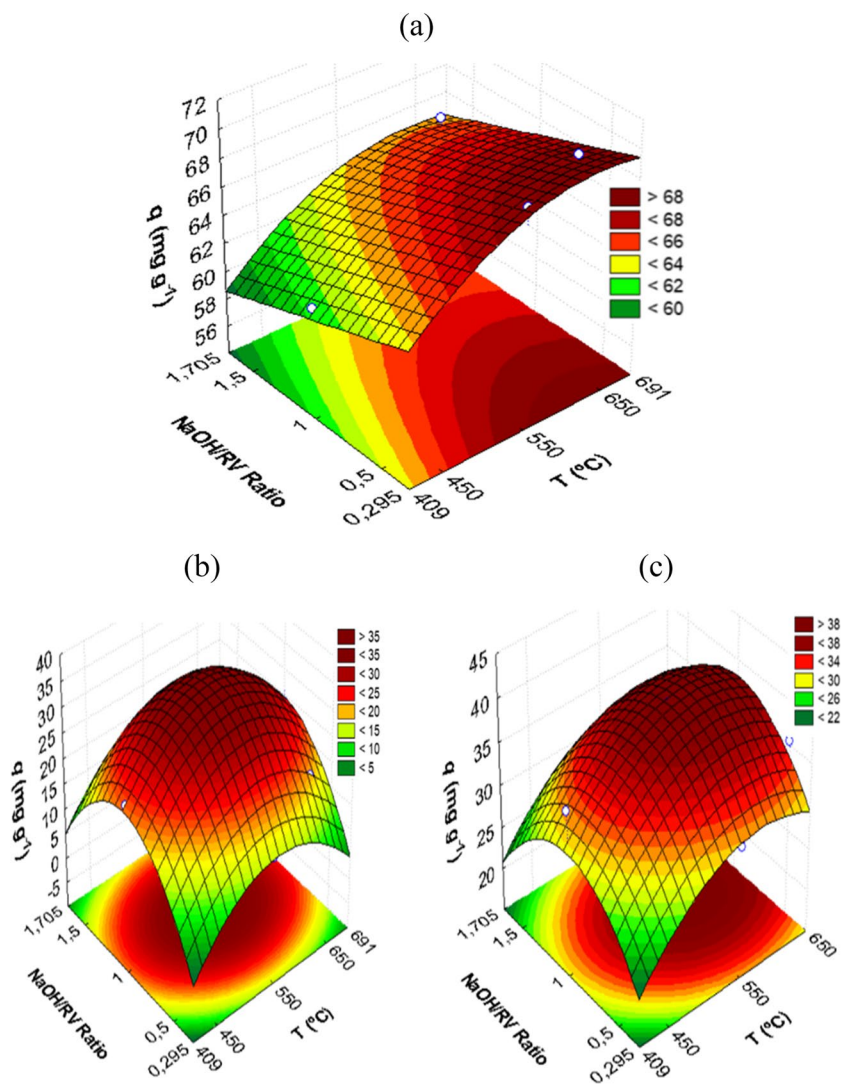
and NaOH/RV ratio = 1.5 ($R = 98.8\%$ and $q = 49.4$ mg g^{-1}). These results were expected considering that there is a significant improvement in the physical properties of the synthesized materials from the increase in T and the NaOH/RV ratio (Table 1S and Fig. 6) of synthesis.

Table 3 compares the sorption capacity of various adsorbents that adsorb different acid red and acid green dyes. This table shows that the NP.F synthesized sample presented greater or very close to the adsorption capacity of the evaluated contaminants. Therefore, it can be suggested that the NP.F sample has a great potential to be adsorbent of the studied dyes.

Adsorption of metal ions

The encoded matrix, real values, independent variables, and responses for the adsorption of Ag$^+$, Co^{2+}, and Cu^{2+} metal ions are shown in Table 4. As in the statistical study of dye adsorption, the confidence interval was 95% ($p <$

0.05). Tables 4S-a and 4S-b show the matrix of experimental design 2^2 and the adsorption capacity (q, expressed in mmol g^{-1}) for the metal ion adsorption tests (Ag$^+$, Co^{2+}, and Cu^{2+}) and the statistical parameters for the equations obtained in the analysis of the dependent variables removal efficiency (R, %) and adsorption capacity (q, mg g^{-1}), respectively.

The Pareto charts for the adsorption capacity response (q, mg g^{-1}) for the adsorption of the metallic ions Ag$^+$ (a), Co^{2+} (b), and Cu^{2+} metallic ions by the NP.F sample are represented in Fig. 9. Regarding the response q for Ag$^+$ (Fig. 9), it was found that the linear and quadratic effects of temperature (T) were significant, as well as the quadratic effect of the NaOH/RV ratio. The negative sign of the linear effect of the NaOH/RV ratio shows that q (mg g^{-1}) increased with the decrease in T. For Co^{2+} (Fig. 9b), all variables were significant ($p < 0.05$). Both linear effects were positive, demonstrating that T and the NaOH/RV ratio affected this response in a directly proportional way in the adsorption of Co^{2+}. Finally, analyzing Fig. 9c, it was possible to verify that only the

Table 5 Adsorption capacities of various adsorbents for de Ag^+, Co^{2+}, and Cu^{2+} ions

Adsorbent	Adsorbate	pH	T (K)	q (mg g^{-1})	References
Colloidal carbon nanospheres	Ag^+	-	298	152.00	
Verde-lodo bentonite		4-5	293	9.72	
Waste coffee grounds		6	298	46.20	
Fly ashes		-	298	39.5	Peres et al. (2022)
Nanocelluloses		3.5-4.5	298	56.0	Liu et al. (2015)
Pectin gel		1	298	67.6	Bhuyan et al. (2018)
NP.F		6.53	298	66.20	This work
Verde-lodo bentonite		4-5	333	6.99	
Pretreated maize husk		5.5	298	35.71	
Nanocelluloses	Cu^{2+}	3.5-4.5	298	20.0	Liu et al. (2015)
Fly ashes		-	298	8.68	Peres et al. (2022)
Hybrid carbon nanocomposites		6	298	40.3	Szewczuk-Karpisz et al. (2021)
Adsorbent	Adsorbate	pH	T (K)	q (mg g^{-1})	References
Biosorbent from Jerivá coconut	Cu^{2+}	5.5	296	15.2	Tochetto et al. (2023)
NP.F		5.98	298	39.70	This work
Organosilicas	Co^{2+}	8	298	37.31	
Alginate nanoparticles		6.5	298	33.56	
Mesoporous carbon		6	298	4.10	
Bottom ashes		-	298	9.7	Peres et al. (2022)
Tectona grandis biochar		5	323	31.2	Vilvanathan and Shanthakumar (2018)
Fibrous chitosan biosorbent		6	298	31.3	Zhuang et al. 2022)
NP.F		6.45	298	34.96	This work

quadratic effect of T and NaOH/RV ratio were significant for the adsorption of Cu^{2+}.

The high values of the coefficient of determination (R^2) and the analysis of calculated and tabulated values for Fischer's F confirm the significance and prediction of the polynomial models, respectively (Table 4S). Therefore, it can be said that the equations found in the statistical analysis were significant, predictive, and reliable. Thus, they can then represent the experimental data of the R and q responses. For example, Fig. 10 represents the equations referring to the adsorption capacity, q, through the response surfaces of the experimental design.

It is possible to verify that the optimization of the adsorption of Ag^+ occurs from an inversely proportional relationship between the T of synthesis and the NaOH/RV ratio of the synthesized materials; that is, the adsorption and removal capacity will be maximum when the T is high, and NaOH/RV ratio is lower (Fig. 10a). The best results were obtained for a ratio of 0.295 and T of 550 °C, with removal capacity, R of 98.3 %, and adsorption capacity, q equal to 69.6 mg g^{-1}. On the other hand, Co^{2+} (Fig. 10b) has its adsorption optimized at the central point when T = 550 °C and NaOH/RV ratio = 1 ($R = 63.1$ % and $q = 34.9$ mg g^{-1}). Finally, the adsorption of Cu^{2+} behaves the same way as that of the cobalt ion, and the maximum values found for q and R were 39.7 mg g^{-1} and 97.1%, respectively. Furthermore,

the adsorption capacity of other materials for the metal ions studied here was compared, and it was verified that NP.F has a good removal effect. This information is shown in Table 5.

Conclusion

Numerous materials were synthesized by alkaline fusion from the residue of volcanic rock powder from the city of Nova Prata, RS, which were obtained from the variation of the ratio of NaOH and volcanic rock and the temperature (T) of synthesis. The synthesis routes were defined based on a preliminary study already published by the authors and the use of an experimental design. In the CCRD 2^2, applied to the experimental adsorptive data for the five contaminants (dye AG 16, dye AR 97, Ag^+, Co^{2+}, and Cu^{2+}) analyzed, the temperature of 550 °C and NaOH/RV ratio equal to 1 were the satisfactory conditions for obtaining high values of adsorption capacity and removal of contaminants, which are in line with the optimization of the physical characteristics of the material, specific surface area, average pore diameter, and total pore volume. In addition, the responses obtained in the experimental design show that the variables temperature and alkalizing/volcanic rock ratio greatly influence the synthesis process of materials, which in turn reflect on the results achieved in the adsorption of contaminants.

For example, the improvement of the specific surface area and the total pore volume of the material depends mainly on the alkalizing/volcanic rock ratio in the material synthesis. In contrast, the mean pore diameter tends to increase and reach the highest values as T increases. Finally, based on the procedure and conditions presented here, it is possible to transform a volcanic rock powder waste into an adsorbent material promising to uptake dyes and metals from water.

Declarations

Ethical Approval Not applicable.

Consent to participate Not applicable.

Consent for publication Not applicable.

Competing interests Guilherme Luiz Dotto is an Environmental Science and Pollution Research associate editor. The other authors declare that they have no competing interests.

References

Ali AA, Shama SA, Amin AS, EL-Sayed SR (2021) Synthesis and characterization of ZrO2/CeO2 nanocomposites for efficient removal of acid green 1 dye from aqueous solution. Mater Sci Eng B Solid-State Mater Adv Technol 269:115167. https://doi.org/10.1016/j.mseb.2021.115167

Aydin H, Baysal G (2006) Adsorption of acid dyes in aqueous solutions by shells of bittim (Pistacia khinjuk Stocks). Desalination 196:248–259. https://doi.org/10.1016/j.desal.2005.11.025

Bhuyan MM, Okabe H, Hidaka Y, Hara K (2018) Pectin-[(3-acrylamidopropyl) trimethylammonium chloride-co-acrylic acid] hydrogel prepared by gamma radiation and selectively silver (Ag) metal adsorption. J Appl Polym Sci 135:1–14. https://doi.org/10.1002/app.45906

Brunauer S, Emmett PH, Teller E (1938) Adsorption of gases in multimolecular layers. J Am Chem Soc. https://doi.org/10.1021/ja01269a023

Bugarčić MD, Milivojević M, Marinković A, Marković B, Sokić M, Petronijević N, Stojanović J (2018) Application of raw volcanic

rock found in Etna valley as an adsorbent of chromates, arsenates and selenates. Metall Mater Eng 24:133–144. https://doi.org/10.30544/366

Chao C, Zhao Y, Song Q, Min J, Wang Z, Ma H, Li X (2019) Volcanic rock-based ceramsite adsorbent for highly selective fluoride removal: function optimization and mechanism. J Chem Technol Biotechnol 94:2263–2273. https://doi.org/10.1002/jctb.6014

Choi JW, Ryu JC, Kwon KS, Song MK, Lee S, Kim SB, Lee SH (2014) Adsorption of ammonium nitrogen and phosphate onto basanite and evaluation of toxicity. Water Air Soil Pollut 225. https://doi.org/10.1007/s11270-014-2059-x

Demir F, Moroydor Derun E (2019) Response surface methodology application to fly ash based geopolymer synthesized by alkali fusion method. J Non Cryst Solids 524:119649. https://doi.org/10.1016/j.jnoncrysol.2019.119649

Duxson P, Fernández-Jiménez A, Provis JL, Lukey GC, Palomo A, Van Deventer JSJ (2007) Geopolymer technology: The current state of the art. J Mater Sci 42:2917–2933. https://doi.org/10.1007/s10853-006-0637-z

Hartmann LA, Medeiros JTN, Baggio SB, Antunes LM (2015) Controls on prolate and oblate geode geometries in the Veia Alta basalt flow, largest world producer of amethyst, Paraná volcanic province, Brazil. Ore Geol Rev 66:243–251. https://doi.org/10.1016/j.oregeorev.2014.11.005

Hosseinzadeh H, Zoroufi S, Mahdavinia GR (2015) Study on adsorption of cationic dye on novel kappa-carrageenan/poly(vinyl alcohol)/montmorillonite nanocomposite hydrogels. Polym Bull. https://doi.org/10.1007/s00289-015-1340-5

Hwang K-J, Hwang MJ, Balathanigaimani MS, Nwe K, Youn Y, Choi W-S, Kim H-A, Nah JW, Shim WG (2019) Adsorption characteristics of light gases on basalt rock-based zeolite 4A. Adsorption 25(4):833–842. https://doi.org/10.1007/s10450-019-00086-6

Jia W, Xiao-Ting C, Hu W et al (2019) Adsorption kinetics research on Chitosan powder Obrilliant crocein. Contemp Chem Res 4:184–185

Kouamo Tchakoute H, Elimbi A, Diffo Kenne BB, Mbey JA, Njopwouo D (2013) Synthesis of geopolymers from volcanic ash via the alkaline fusion method: Effect of Al2O3/Na2O molar ratio of soda–volcanic ash. Ceram Int 39(1):269–276. https://doi.org/10.1016/j.ceramint.2012.06.021

Liu P, Borrell PF, Božič M, Kokol V, Oksman K, Mathew AP (2015) Nanocelluloses and their phosphorylated derivatives for selective adsorption of Ag+, Cu2+ and Fe3+ from industrial effluents. J Hazard Mater 294:177–185. https://doi.org/10.1016/j.jhazmat.2015.04.001

Masoudian N, Rajabi M, Ghaedi M, Asghari A (2018) Highly efficient adsorption of naphthol green B and phenol red dye by combination of ultrasound wave and copper-doped zinc sulfide nanoparticles loaded on pistachio-nut shell. Appl Organomet Chem 32:1–13. https://doi.org/10.1002/aoc.4369

Monz'on JD, Gonzalez MR, Mardones LE, Conconi MS, Pereyra AM, Basaldella EI (2019) The role of alkaline activation in the structural transformations of aluminosiliceous industrial wastes towards zeolite production. Mater Today Commun 21:100624. https://doi.org/10.1016/j.mtcomm.2019.100624

Myers RH, Montgomery DC, Anderson-Cook CM (2009) Response surface methodology: process and product optimization using designed experiments, 3rd edn. John Wiley & Sons. John Wiley & Sons, New Jersey

Ontiveros-Cuadras JF, Ruiz-Fernández AC, Sanchez-Cabeza JA, Pérez-Bernal LH, Preda M, Páez-Osuna F (2018) Mineralogical signatures and sources of recent sediment in a large tropical lake. Int J Sediment Res 33:183–190. https://doi.org/10.1016/j.ijsrc.2017.12.002

Pejman A, Nabi Bidhendi G, Ardestani M, Saeedi M, Baghvand A (2015) A new index for assessing heavy metals contamination in

sediments: A case study. Ecol Indic 58:365–373. https://doi.org/10.1016/j.ecolind.2015.06.012

Peres EC, Netto MS, Mallmann ES, Silva LFO, Foletto EL, Dotto GL (2022) Synthesis of geopolymers from fly and bottom ashes of a thermoelectrical power plant for metallic ions adsorption. Environ Sci Pollut Res 29:2699–2706. https://doi.org/10.1007/s11356-021-15882-3

Pinto VM, Hartmann LA (2011) Flow-by-flow chemical stratigraphy and evolution of thirteen Serra Geral Group basalt flows from Vista Alegre, southernmost Brazil. An Acad Bras Cienc 83:425–440. https://doi.org/10.1590/S0001-37652011000200006

Remor MB, Sampaio SC, de Rijk S, Vilas Boas MA, Gotardo JT, Pinto ET, Schardong FA (2018) Sediment geochemistry of the urban Lake Paulo Gorski. Int J Sediment Res 33:406–414. https://doi.org/10.1016/j.ijsrc.2018.04.009

Rossatto DL, Netto MS, Reis GS, Silva LFO, Dotto GL (2022) Volcanic rock powder residues as precursors for the synthesis of adsorbents and potential application in the removal of dyes and metals from water. Environ Sci Pollut Res 29:25685–25693. https://doi.org/10.1007/s11356-021-17749-z

Silva PRB, Makara CN, Munaro AP, Schnitzler DC, Wastowski AD, Poleto C (2016) Comparison of the analytical performance of EDXRF and FAAS techniques in the determination of metal species concentrations using protocol 3050B (USEPA). Int J River Basin Manag 14:401–406. https://doi.org/10.1080/15715124.2016.1203792

Szewczuk-Karpisz K, Wiśniewska M, Medykowska M, Galaburda MV, Bogatyrov VM, Oranska OI, Błachnio M, Oleszczuk P (2021) Simultaneous adsorption of Cu(II) ions and poly(acrylic acid) on the hybrid carbon-mineral nanocomposites with metallic elements. J Hazard Mater 412. https://doi.org/10.1016/j.jhazmat.2021.125138

Tchadjié LN, Djobo JN, Ranjbar N, Tchakouté HK, Kenne BD, Elimbi A, Njopwouo D (2016) Potential of using granite waste as raw material for geopolymer synthesis. Ceram Int 42(2):3046–3055. https://doi.org/10.1016/j.ceramint.2015.10.091

Thommes M (2010) Physical adsorption characterization of nanoporous materials. Chem Ing Tech. https://doi.org/10.1002/cite.201000064

Tochetto GA, Brandler D, Pigatto J, Pasquali GDL, de Almeida Alves AA, Kempka AP, da Luz C, Dervanoski A (2023) Kinetic modeling of the adsorption and desorption of metallic ions present in effluents using the biosorbent obtained from Syagrus romanzoffiana. Environ Monit Assess 195. https://doi.org/10.1007/s10661-023-11459-4

Vieira Y, Netto MS, Lima ÉC, Anastopoulos I, Oliveira MLS, Dotto GL (2021) An overview of geological originated materials as a trend for adsorption in wastewater treatment. Geosci Front 13:101150. https://doi.org/10.1016/j.gsf.2021.101150

Vilvanathan S, Shanthakumar S (2018) Ni2+ and Co2+ adsorption using Tectona grandis biochar: kinetics, equilibrium and desorption studies. Environ Technol (United Kingdom). https://doi.org/10.1080/09593330.2017.1304454

Vosoogh A, Saeedi M, Lak R (2016) Heavy metals relationship with water and size-fractionated sediments in rivers using canonical correlation analysis (CCA) case study, rivers of south western Caspian Sea. Environ Monit Assess 188. https://doi.org/10.1007/s10661-016-5611-x

Wajima T, Oya K, Shibayama A, Sugawara K, Munakata K (2011) Synthesis of hydrocalumite-like adsorbent from blast furnace slag using alkali fusion. ISIJ Int 51(7):1179–1184. https://doi.org/10.2355/isijinternational.51.1179

Wang Q, Liang L, Xi F, Tian G, Mao Q, Meng X (2020) Adsorption of Azo Dye Acid Red 73 onto Rice Wine Lees: Adsorption Kinetics and Isotherms. Adv Mater Sci Eng 2020. https://doi.org/10.1155/2020/3469579

Wdowin M, Franus M, Panek R, Badura L, Franus W (2014) The conversion technology of fly ash into zeolites. Clean Technol Environ Policy. https://doi.org/10.1007/s10098-014-0719-6

Wei N, Wang XL, Guan WX, Guo YG (2014) Characterization of a novel zeolite synthesized from coal fly ash. Adv Mat Res 886:84–87

Xing Z, Tang B, Chen X, Fu F, Zhang Z, Lu Z (2014) Adsorption mechanism of acid red 73 onto magnetic nanoparticles Fe3O4 from aqueous phase. Acta Sci Circumst 4:2246–2255

Zhuang S, Zhu K, Xu L, Hu J, Wang J (2022) Adsorption of Co2+ and Sr2+ in aqueous solution by a novel fibrous chitosan biosorbent. Sci Total Environ 825:153998. https://doi.org/10.1016/j.scitotenv.2022.153998